Ultrasound induced hydrogen release from ammonia borane mediated by oxidized multiwalled carbon nanotube under hydrolytic conditions

Applied Surface Science 717 (2026) 164800

Contents lists available at ScienceDirect

Applied Surface Science

journal homepage: www.elsevier.com/locate/apsusc

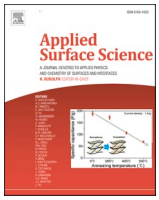

Full Length Article

Ultrasound induced hydrogen release from ammonia borane mediated by oxidized multiwalled carbon nanotube under hydrolytic conditions

Mattia Bartoli [a,b,*], Marco Etzi [a,b], Stefania Lettieri [c], Giuseppe Ferraro [c], Candido Fabrizio Pirri [a,c], Sergio Bocchini [a,b,c]

[a] Center for Sustainable Future Technologies—CSFT@POLITO, Via Livorno 60, 10144 Torino, Italy
[b] Consorzio Interuniversitario Nazionale per la Scienza e Tecnologia dei Materiali (INSTM), Via G. Giusti 9, 50121 Florence, Italy
[c] Politecnico di Torino, Department of Applied Science and Technology, C.so Duca degli Abruzzi 24, 10129 Turin, Italy

ARTICLE INFO

Keywords:
Ammonia borane
Hydrogen storage
Reactivity
Chemical bonded hydrogen

ABSTRACT

The field of hydrogen storage is one of the last frontiers in the exploitation of hydrogen-based technology. Particularly, the utilization of ammonia borane is a very promising route to solve the issue related to hydrogen storage due to the content of hydrogen up to 19.8 wt% and the stability in the ambient temperature and pressure conditions. Nevertheless, the hydrogen release from ammonia borane is quite complex under thermal stimuli, with several secondary compounds released. Alternatively, hydrolysis of ammonia borane is a simpler route to release of hydrogen in presence of water without any side reaction when a catalyst is used. This study investigates the ultrasound-assisted hydrolytic dehydrogenation of ammonia borane mediated by oxidized multiwalled carbon nanotubes (MWCNTs) as a metal-free energy-efficient catalytic system. The application of ultrasonic irradiation significantly enhanced the catalytic performance by promoting mass transport, improving water molecule activation, and increasing the dispersion and reactivity of the oxidized MWCNTs in the water medium. The oxidized MWCNTs promote the activation of ammonia borane, reducing the activation energy of the systems over 77% and reaching a remarkable hydrogen release efficiency with a conversion of up to 98%.

1. Introduction

The hydrogen production is a very vital sector that has reached considerable achievements during the years, earning a reputation for solidity and trustworthiness [1]. As far as its production is concerned, hydrogen has been the subject of intense research aimed at improving production systems, achieving significant advances in the field of sustainable production through electrolysers [2–5], but hydrogen storage under both compressed and liquid phase remains the great unsolved issue in the field due to technological constraints [6]. Large hydrogen volumes are stored as liquid hydrogen in expensive, insulated vessels [7], where some amount of the stored product is lost through evaporation. Accordingly, the use of liquid hydrogen is limited to those applications, which are requiring high volume and pure gas, such as chemical and aerospace industries. For the small-scale hydrogen storage, there are plenty of different technologies, but all of them manifest some intrinsic weakness. Compressed hydrogen has been traditionally tested as viable solution for mobility, but the hydrogen tank technology faces technical problems due to hydrogen diffusivity and volumetric energy content [8]. Hydrogen diffusivity through several metal alloys could cause tank embrittlement and crack formation with hydrogen leaks rising major safety issues [9]. Furthermore, the energy content of compressed hydrogen per unit volume is comparable to that of methane, and it is four orders of magnitude lower than that of liquid fuels. An interesting combination of pressurized and liquid store methodology is represented by the so-called cold-cryo compression [10]. This technique is based on the storage of hydrogen under cryogenic/cycling temperatures ranging from –233 °C up to 193 °C, under pressure in the range between 250–300 bar. Cold-cryo compression route tanks are highly insulated, and they are made to withstand high internal pressure. Nevertheless, the storage cost is prohibitive, reaching up to 395 €/kg, besides requiring complex engineering solutions [11]. Alternatively, hydrogen could be physisorbed onto several classes of materials ranging from carbon [12,13] to inorganic materials (i.e., zeolites) [14] and metal organic frameworks (MOFs) [15] through Van der Waals force interaction under moderate pressure (30 bar) and low temperature (−193 °C). However, physisorption is governed by Chahine's rule [16] that states the limit of 1 wt% of adsorbed hydrogen for every 500 m^2/g of surface area, limiting

* Corresponding author.

https://doi.org/10.1016/j.apsusc.2025.164800
Received 30 July 2025; Received in revised form 1 October 2025; Accepted 2 October 2025
Available online 2 October 2025

the hydrogen storage capability. Furthermore, it was reported a decrease in the isosteric heat of adsorption, suggesting the saturation of strong adsorption sites [17]. In a different way, hydrogen could be stored as chemically bonded hydrogen into organic, metalorganic, and inorganic compounds. This storage strategy is called chemically stored hydrogen and represents a vast, not fully explored area in the field of hydrogen storage. Hydrogen could be entrapped into simple molecules such as methane [18,19] or ammonia [20], but its release is not straightforward [23]. Alternatively, liquid organic hydrogen carriers represent a class of compounds, such as N-ethylcarbazole derivatives [21], characterized by a high regenerability and high gravimetric hydrogen storage (GHS) capacity up to 22.1 wt% [22]. Nevertheless, the use of liquid organic hydrogen carriers requires the massive use of noble metals for releasing/incorporating hydrogen, and they can prove quite risky for human safety [23]. Hydrogen could also be chemically stored in inorganic hydrides such as $LiBH_4$ or magnesium hydrides, reaching a GHS ranging from 14.9 wt% up to 18.5 wt% with a volumetric energy density up to 17.6 MJ/l [24]. Despite these interesting properties, inorganic hydrides are difficult to regenerate and sensitive to water [25,26]. A more promising and viable chemical hydrogen pathway involves the use of organic species such as amine-boranes as hydrogen carriers. These species, particularly ammonia borane (AB) [27], have been widely used both for releasing hydrogen through thermolysis [28–30] or hydrolysis [31–33]. The theoretical gravimetric hydrogen storage capacity (GHS) reaches up the remarkable value of 19.6 wt%, but the hydrogen release mechanism is quite complex and involves the release of complex borazane species [34]. This represented a considerable drawback considering the high purity of hydrogen required for applications such as fuel cells and poor regenerability, while AB hydrolysis represents a simpler approach with a reduced GHS. Nevertheless, it requires both the presence of catalysts including metal [35–39], organic [40] and inorganic species [41–46] and the apport of energy [47]. In this work, we exploited a new approach combining a simple acidic catalyst based on a stable acidic materials, the oxidized multiwalled carbon nanotubes (MWCNTs), under ultrasound irradiation. The ultrasound mediated hydrolysis allowed to maximize the energy efficiency of the systems and realizing a switchable system able to turn on–off by simple removal of ultrasound stimuli.

2. Materials and methods

2.1. Materials

MWCNTs (NC7000TM, produced via the Catalytic Chemical Vapor Deposition (CCVD) process) were purchased from Nanocyl SA (Sambreville, Belgium). They have a carbon purity of 90 % and a surface area of 250–300 m^2/g, as reported in the datasheet provided by the supplier. Nitric (63 %) and sulphuric acid (>95 %) were purchased from Sigma-Aldrich and used without any further purification.

2.2. Preparation of oxidized MCNTs

MWCNTs were preliminary annealed at 1600 °C for 1 h in inert atmosphere in order to remove impurities, providing a homogenous benchmark for the further oxidative modifications [48], producing the sample named 0CNTs.

Oxidation of annealed MWCNTs was run accordingly to the procedure reported in Bartoli et al. [29]. 200 mg of CNTs were suspended into 15 mL solution of sulphuric acid and nitric acid with a volume ratio of up to 3 and sonicated in an ultrasound bath at 60 °C for 60 min. The resulting suspension was diluted with deionized water and filtered. The solids recovered were washed several times with deionized water and dried at 50 °C in vacuum for 16 h.

2.3. Characterization of 0CNTs and 60CNTs

0CNTs and 60CNTs were analyzed through Raman spectroscopy using a Renishaw inVia (H43662 model, Gloucestershire, UK) equipped with a green laser line (514 nm) with a 50 × objective. Raman spectra were recorded in the range from 500 to 4000 cm^{-1}. Signals were fitted according to the methodology proposed by Tagliaferro et al. [49].

The surface functionalities were investigated by using X-ray photoelectron spectroscopy (XPS) using a PHI 5000 Versaprobe Physical Electronics (Chanhassen, MN, USA) scanning X-ray photoelectron spectrometer (monochromatic Al K-alpha X-ray source with 1486.6 eV energy, 15 kV voltage, 1 mA anode current).

0CNTs and 60CNTs were analyzed through FT-IR (ATR mode) spectroscopy using a TENSOR II spectrometer (Bruker) equipped with a ATR module Platinum II (Bruker).

Morphology of 0CNTs and 60CNTs was investigated through a Field Emission Scanning Electron Microscope (FE-SEM) Zeis SupraTM 25 (Oberkochen, Germany).

XRD patterns were acquired by using a Panalytical diffractometer (X'PERT PRO PW3040/60 Almelo, The Netherlands). with a Cu K α radiation at 40 kV and 40 mA as X-Ray source. The diffraction patterns were obtained from RM powder in the 2θ range from 20° to 40° (step size of 0.013°).

Stability of xCNTs materials was investigated through thermogravimetric analysis (TGA) using Netzsch TG 209F1 Libra in N2 flux (20 mL/min) with a temperature ramp of 10 °C/min from 30 to 800 °C.

2.4. AB hydrolytic test for hydrogen evolution

AB hydrolysis was carried out at different temperatures (30, 40, and 50 °C) in nitrogen atmosphere under ultrasound irradiation using a thermostat bath (ElmasonicP 60 Hz, 280 W). 0CNTs or 60CNTs was put in a two-necked round-bottom flask connected to a gas burette and to a pressure-equalized funnel and sonicated for 10 min. Then, AB was added reaching a final concentration of up 0.5 M. using xCNTs/AB (x = 0 or 60) of 0, 2, and 5 wt%. The hydrogen evolution was monitored using the gas burette, adjusting by considering the external pressure and temperature. After the reaction was ended, the catalyst was recovered by filtration, dried at 50 °C and 20 mbar until constant weight prior to being reused and characterized. Each catalytic test was run twice without observing detectable changes in the conversion results.

Kinetic constants (k) for each reaction were obtained by fitting the conversion vs time plot using a pseudo-first-order model [50], and activation energies (E_a) were calculated by using Arrhenius equation [51].

3. Results and discussion

3.1. Characterization of 0CNT and 60CNT

0CNT and 60CNT were analyzed through TGA in order to quantify the functionalities introduced through the oxidation process as reported in Fig. 1 and summarized in Table 1.

0CNTs did not show any appreciable thermal degradation up to 800 °C when residual oxygens formed after exposure of 0CNT to the air were degraded, leading to a residual mass of up to 98.9 %. Contrary, the 60CNTs showed significant degradation steps across the temperature range investigated as reported by Chernyak et al. [52]. 60CNT showed a T_{onset} around to 120 °C due to water desorption and a first degradative stage at 155 °C due to the loss of carboxylic residues that were 1.9 wt%. The further degradative process involved the release of hydroxylic and carbonyl moieties that are 9.6 wt%.

As shown in Fig. 2 a, the FT-IR (ATR mode) spectra of fresh 0CNT did not show any appreciable signal as a consequence of the annealing processes. Fresh 60CNTs showed the presence of carboxylic and carbonyl residues as proved by $\nu_{C=O}$ at around 1700–1713 and 1680

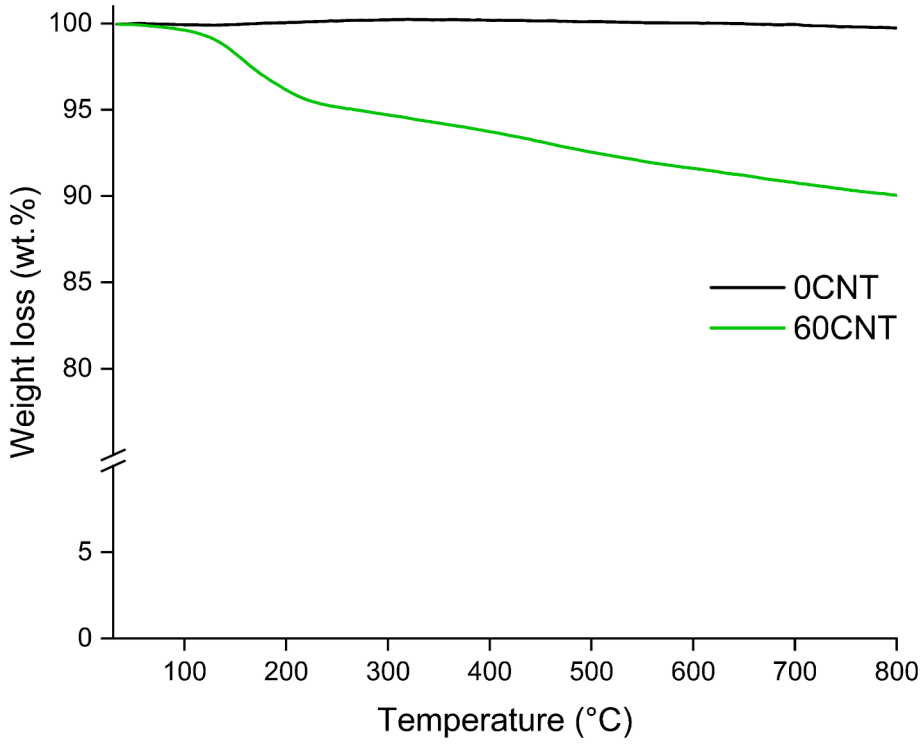

Fig. 1. TGA analysis of 0CNT (black line) and 60CNT (green line) in temperature range from 30 to 800 °C.

Table 1
TGA of 0CNT and 60CNT in N_2 atmosphere in the range from 30 °C up to 800 °C.

Sample	T_{onset} (°C)	T_{max1} (°C)	Residue @ T_{max1} (%)	T_{max2} (°C)	Residue @ $T_{max\ 2}$ (%)	Residue @ 800 °C (%)
0CNTS	–-	––	––	––	––	98.9
60CNTs	120	155	98.1	185	94.1	89.6

cm^{-1}, hydroxylic residues as proved by the presence of the broad ν_{OH} band from 3000-3500 cm^{-1}, and other oxygen-based functionalities as proved by the presence of $\nu_{C\text{-}O}$ (1520 cm-1) and $\delta_{C\text{-}O}$ (1325 cm-1) bands. As shown in Fig. 2 b, the Raman spectra of fresh 0CNTs showed a well-defined D and G peaks centered at 1336 cm^{-1} and 1575 cm^{-1}, respectively [53], while 2D region is composed of three peaks known as 2D, D + G, 2D centered at 2240, 2680, and 3896 cm^{-1}, respectively. Fresh 60CNTs showed negligible shift in the peaks position but a I_D/I_G ratio of 0.6 compared with 0.4 of fresh 0CNT, with a volumetric crystallite L_a that decreased from 37.2 down to 25.4 nm [54]. The decrement of crystallinity was in good agreement with the oxidative process that induces the formation of defects into the sp^2 structure of MWCNTs, as also proved by the comparison of two components in the G peak of 60CNT (supporting information Fig. S1 b and d) absent in 0CNT (supporting information Fig. S1 a and c). As reported by Shimoidara et al. [55], the G^1 component was due to the graphitic domains with a high order of bond angle, while G^2 arose from amorphous disordered domains. The ratio between G^1 and G^2 is a valuable tool to evaluate bond angle disorder: 60 CNT is characterized by a value of 9.4, still far higher than non-annealed carbon species, supporting the introduction of oxygen residues

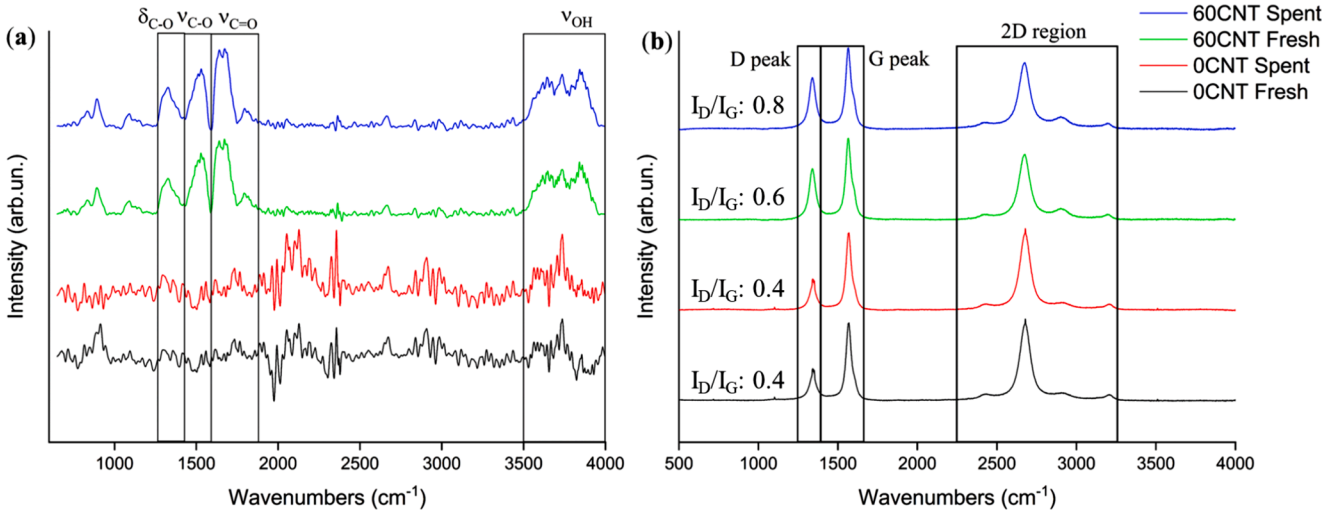

Fig. 2. Spectroscopical investigation through (a) FT-IR (ATR mode) and (b) Raman spectroscopy in the range from 500 up to 4000 cm^{-1} of fresh 0CNT (black line), spent 0CNT (red line), 60 CNT (green line), and spent 60CNT (blue line).

without compromising too much the carbon structure itself [55–65] (as also shown by XRD reported in Fig. 3).

As shown in Fig. 3, the diffraction patterns of both 0CNT and 60CNT showed a broad diffraction peak centred at 25.95° as reported by Tai et al. [66], in agreement with MWCNTs annealed at temperatures lower than 2000 °C. As reported in supporting information (Fig. S2), the asymmetry of 002 diffraction peak can be attributed to a diffraction peak centred at around 24.81°related to MWCNTs bundles as reported by Futaba et al. [67].

A more detailed investigation about both 0CNT and 60 CNT was run though XPS analysis as shown in Fig. 3 and summarized in Table 2.

As shown in Fig. 4 and b and summarized in Table 2, 0CNT did not show the presence of carboxylic functionalities in both C 1 s and O 1 s spectra, while the presence of traces of oxygen species (hydroxyls 72 %, 532.4 eV; carbonyls 28 %, 533.7 eV) was introduced after the exposition of 0CNT to the atmosphere. The oxidation process of 0CNT introduced carboxylic functionalities up to 6 % (289.9 eV) together with the massive increment of both hydroxylic and carboxylic species with a decrement of C sp^2 down to 66 % from 88 %.

As shown in Fig. 5 a, the FESEM-EDX analysis of 0CNT showed a very entangled bundles in agreement with the XRD analysis with MWCNTs longer around 20 μm and a thickness of up around 30 nm while the oxidation process did no significantly affected the morphology of 60CNT as shown in Fig. 5b while the elemental analysis confirmed the oxidation with the oxygen amount that rose up to 4.3 wt%.

3.2. Catalytic ultrasound AB hydrolysis mediated by 60CNTs

The AB hydrolysis was studied using an ultrasound-mediated bath using several temperatures as reported in Fig. 6 and summarized in Table 3 with a reaction pathway as the one reported in Eq. (1).

$$NH_3BH_3 + 2H_2O \rightarrow NH_4BH_2 + 3H_2 \quad (1)$$

As shown in Fig. 6 and summarized in Table 3, the hydrolysis of AB in presence of water showed conversion ranging from 12.2 % at 30 °C up to 18.3 % at 50 °C, showing a moderate effect of temperature on the process. As reported by Gianola et al. [32], the results of thermal-mediated hydrolytic test were comparable with the ultrasound-mediated one, reaching a conversion of 17.3 %. The addition of 0CNT slightly affected the conversion rate reaching a conversion of 23.8 % at 50 °C, suggesting that the surface of neat MWCNTs promotes a destabilization of N-B bonds under ultrasound irradiation, as reported by Wu et al. [68].

The utilization of 60CNT drastically increased the conversion rate, reaching up 62.1 % at 30 °C and a near complete conversion after 600 s (98.7 %) at 50 °C. As discussed by Sanyal et al. [31], the heterogenous acid-mediated hydrolysis of AB involved a preliminary step of adsorption on the acidic site with the protonation of $-BH_3$ lowering the activation energy the bond dissociation energy promoting the insertion of water molecules, hydrogen release and NH_4BO_2 production.

Accordingly, we observed a reduction of E_a from 160.4 kJ/mol for the non-catalyzed system down to 133.6 kJ/mol in presence of 0CNTs. The E_a decrement of 17 % was reasonably the adsorption phenomena on the surface of non-oxidized MWCNTs, while the use of 60CNT further reduced the E_a of 77 % down to 36.6 kJ/mol. Additionally, the use of 60CNT boosted the kinetics of the reaction reaching a k of 4.4 s^{-1} at 50 °C that was three orders of magnitude higher than the others proving the high activity of acid sites that showed TON of up to 4.8 * 10^4 at 50 °C.

Table 2
Summary of XPS chemical features of fresh/spent 0CNT and 60CNT.

Sample	Chemical functionalities (%)						
	Carbon				*Oxygen*		
	***C* sp^3**	***C*-O**	***C*=O**	***C*OOH**	***C*-O**	***C*=O**	***C*OOH**
0CNT[a]	88	8	4	0	72	28	0
60CNT[a]	66	18	10	6	63	27	10
0CNT[b]	92	7	1	0	71	29	0
60CNT[b]	68	19	6	7	65	26	11

[a]) Fresh material.
[b]) Spent material.

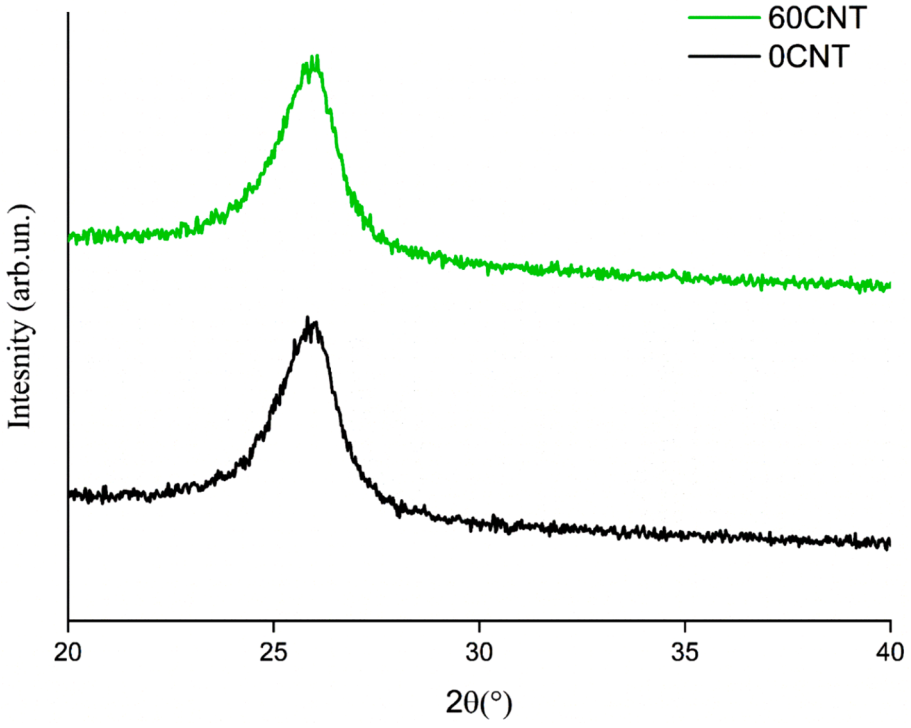

Fig. 3. XRD analysis of 60CNT (black line) and spent 60CNT (green line).

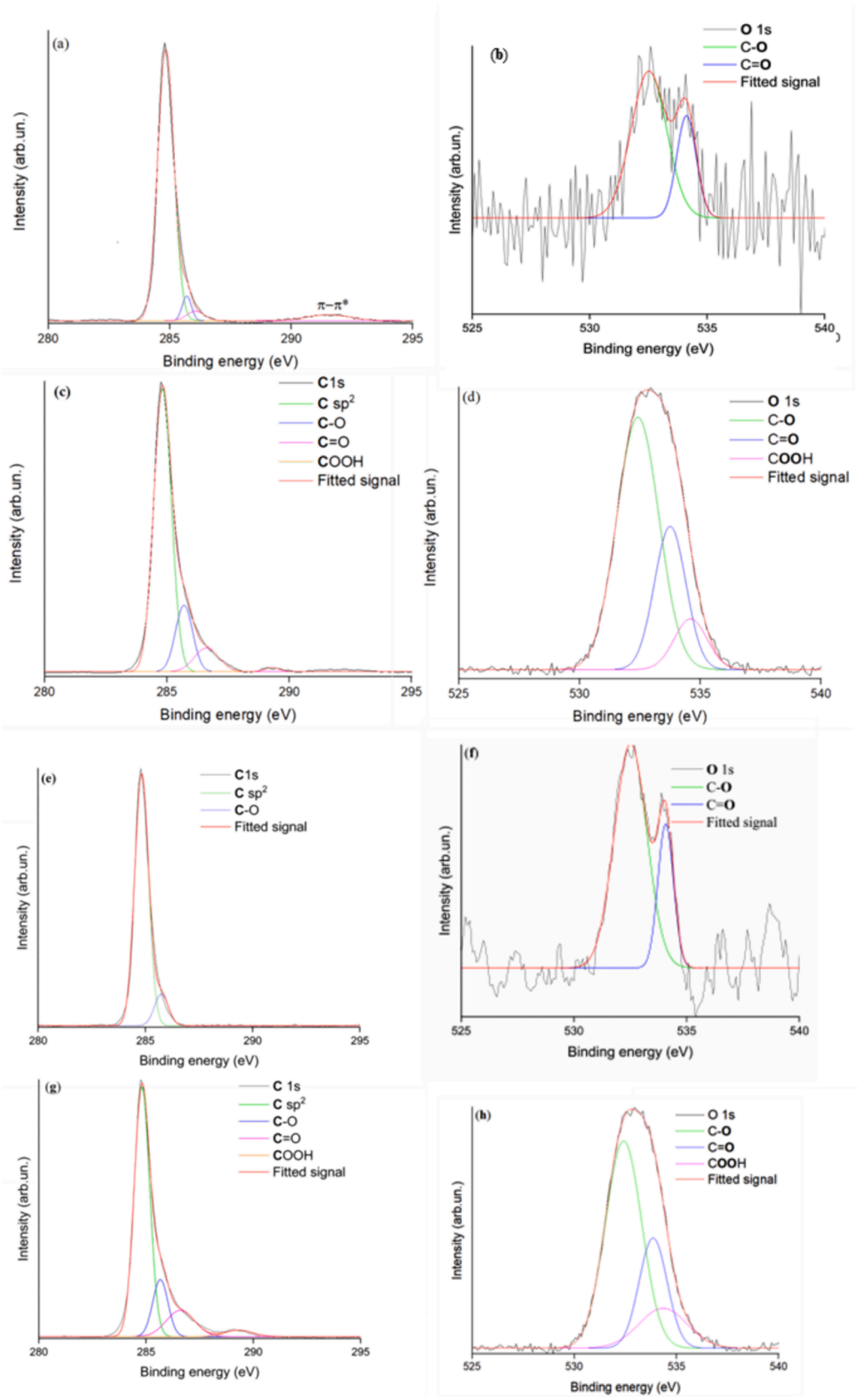

Fig. 4. XPS analysis of investigation of fresh 0CNT (a C1s, b O1s), spent 0CNT (c C1s, d O1s), 60CNT (e C1s, f O1s), 60CNT (g C1s, h O1s),

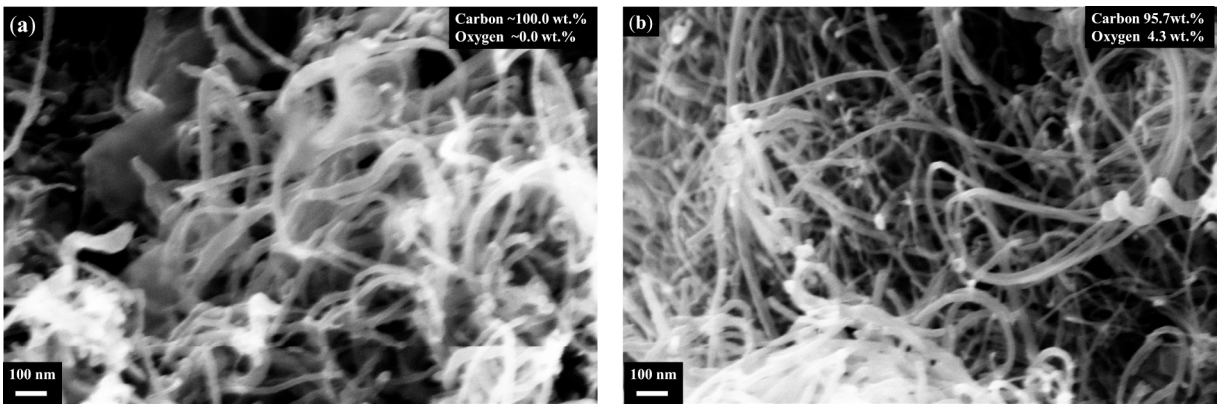

Fig. 5. FESEM pictures of (a) 0CNT and (b) 60CNT.

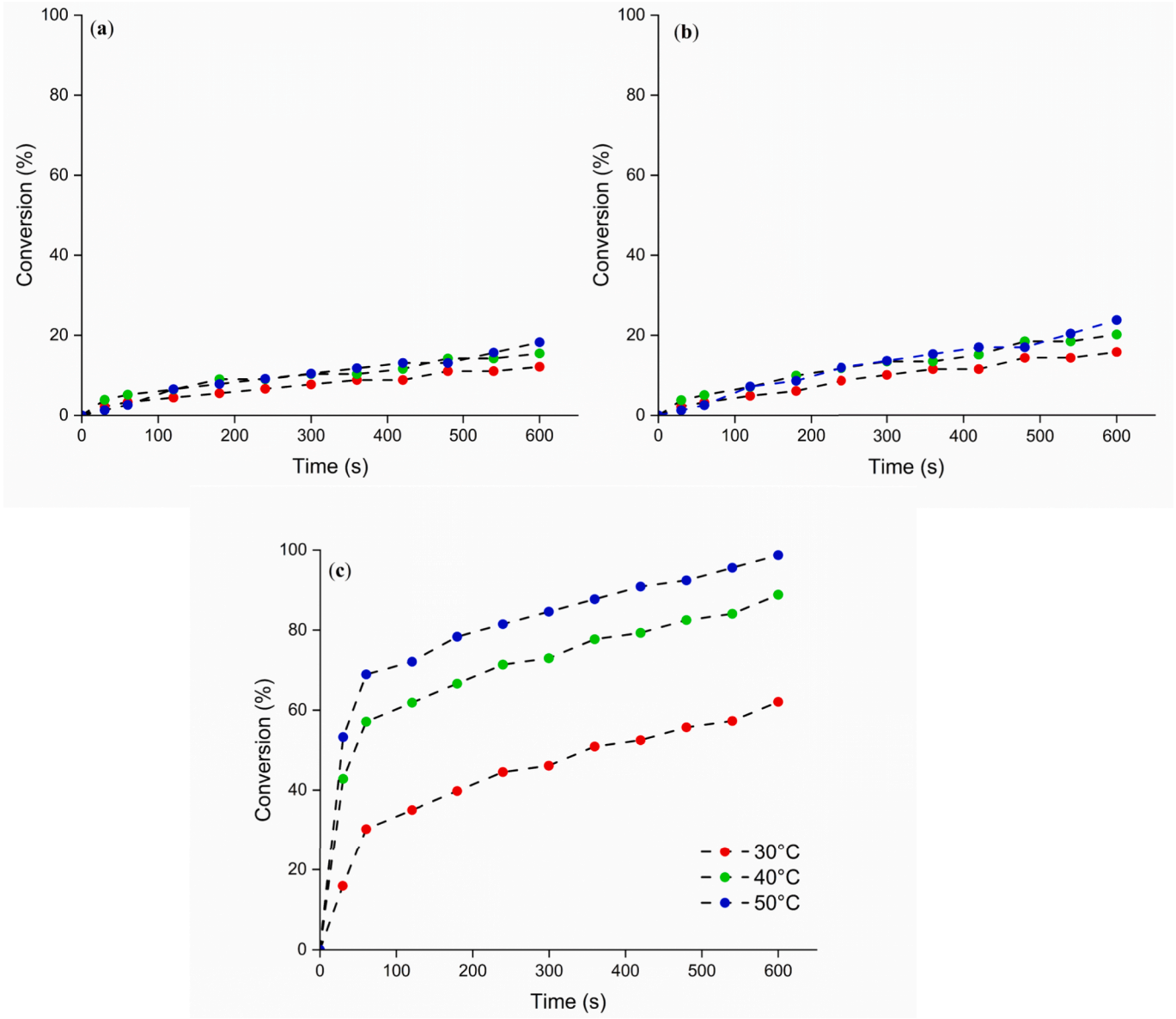

Fig. 6. Ultrasound mediated hydrolysis of AB (a) without any catalyst and in presence of 2 wt% of (b) 0CNT and (c) 60CNT at different temperatures.

Table 3
AB hydrolysis outputs calculated from catalytic tests.

	Conversion (%)			k (s^{-1})			Turn over number (TON)[a]		Ea (kJ/mol)	
	30 °C	*40 °C*	*50 °C*	*30 °C*	*40 °C*	*50 °C*	*30 °C*	*40 °C*	*50 °C*	
Water	12.2	15.5	18.3	$0.9*10^{-3}$	$1.1*10^{-3}$	$1.2*10^{-3}$	n.a.	n.a.	n.a.	160.4
0CNT	15.8	20.1	23.8	$1.1*10^{-3}$	$1.3*10^{-3}$	$1.4*10^{-3}$	n.a.	n.a.	n.a.	133.6
60CNT	62.1	88.9	98.7	2.1	3.8	4.4	$3.0*10^{4}$	$4.4*10^{4}$	$4.8*10^{4}$	36.6

[a]) TON was calculated as follow: mol of converted AB/mol COOH, mol of COOH were calculated based on the COOH wt.% of 60CNTs.

As shown by the data reported, AB hydrolysis showed a clear temperature dependence in accordance with the the heterogeneous acid-mediated mechanism of N-B cleavage [40]. The increment of temperature promoted a multiple step-process involving the adsorption of AB on both carbon surface and acidic sites of 60CNTs with the protonation of the $–BH_3$ unit lowering the bond dissociation energies and the insertion of water leading to the formation H-H bonds. The temperature also promoted a faster desorption fo the products reporterd in eq.1 fromt eh surface of the 60CNT [69].

As shown in Fig. 7, the utilization of 1 wt% of 60CNT decreased the k of the reaction down to 3.3 s^{-1} at 50 °C, while a further increment up to 5 wt% only slightly increased k up to 4.7 s^{-1} at 50 °C, leaving the conversion at the same value after 600 s.

As shown in Fig. 8, 60CNT showed a good stability across five catalytic cycles without any appreciable variations. As shown in Fig. 2 a, 0CNT and 60CNT did not show any residue due to AB hydrolysis products nor further modification, as also emerged from the XPS analysis of spent materials reported in Table 2. Raman spectrum of spent 60CNT (Fig. 2 b) showed a small appreciable increment of I_D/I_G reasonably due to the rearrangement of the MWCNTs bundles due to the water adsorption and removal.

We further compared the catalytic performances of 60CNT for AB hydrolysis with those found in the literature for the same reaction based on metal catalyst. As shown in Table 4, 60CNT showed a ΔE_a comparable with the one achieved by using noble Ni [70] and Ru [71] supported onto MWCNTs while was lower than PtO supported on MWCNTs [72]. Nevertheless, the presence of noble metal reduced the conversion time [73,74] while the use of cheap metals [75] such as copper or waste based materials [33,76]let to comparable results. Interestingly, the utilization of ultrasound mediated conditions seemed to stimulate the activity of carboxylic residues probably due to a a combination of mass transport and ultracavitaiton phenomena [77,78].

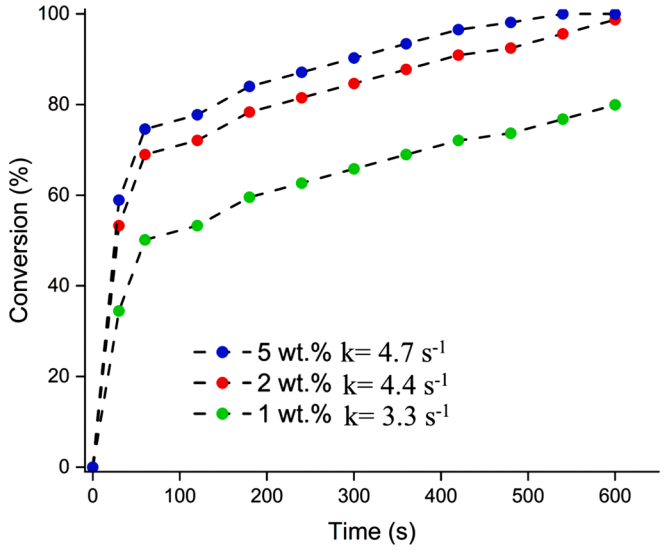

Fig. 7. Ultrasound-mediated hydrolysis of AB with 1, 2, and 5 wt% 60CNT at 50 °C.

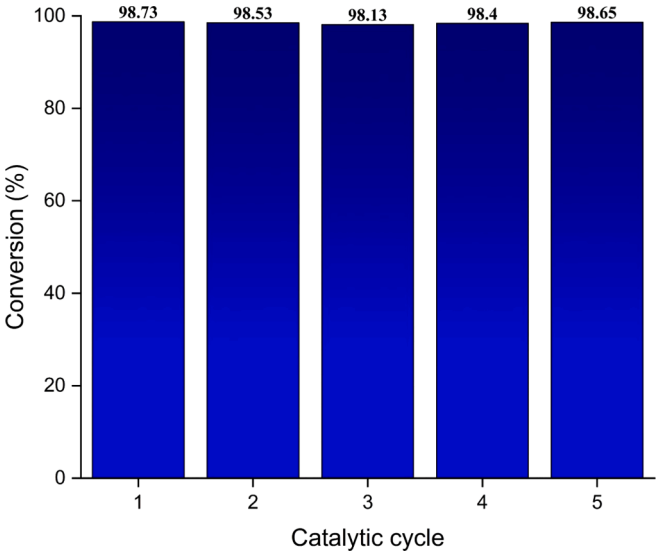

Fig. 8. Ultrasound-mediated hydrolysis of AB using 5 wt% 60CNT at 50 °C for five catalytic cycles.

4. Conclusions

In this work, we demonstrated that the combination of an acidic supported catalyst together with the ultrasound technique provide an effective metal-free platform for the hydrolytic release of hydrogen from AB under very mild conditions. The introduction of surface oxygen-containing functional groups, in particular carboxylic residues, onto the MWCNTs significantly enhanced their catalytic activity by promoting adsorption of AB and reducing the E_a over 77 % reaching a conversion over 98 %. Ultrasound irradiation played a critical role in further improving the system performance by accelerating mass transfer, increasing the contact between AB and the active site, and enhancing the desorption of products after hydrogen release. Furthermore, the utilization of ultrasound stimuli allowed to trigger with an on–off hydrogen release by simply removing the ultrasound source, considering the negligible hydrogen release from AB without external stimuli.

These results highlight the synergistic role of surface-functionalized MWCNTs and ultrasonic irradiation in promoting efficient, sustainable hydrogen generation from AB development of scalable, environmentally benign hydrogen production systems based on lightweight, non-metallic catalysts under mild operating conditions.

CRediT authorship contribution statement

Mattia Bartoli: Writing – review & editing, Writing – original draft, Visualization, Supervision, Methodology, Investigation, Formal analysis, Data curation, Conceptualization. **Marco Etzi:** Writing – review & editing, Writing – original draft, Visualization, Investigation, Formal analysis, Data curation. **Stefania Lettieri:** Writing – review & editing, Writing – original draft, Visualization, Validation, Formal analysis, Data curation. **Giuseppe Ferraro:** Writing – review & editing, Writing –

Table 4
Comparison of catalytic performance of 60CNT under ultrasound stimuli and other catalytic systems.

Catalyst	Particle size (nm)	Conversion (%)	t (min)	ΔE_a (kJ mol^{-1})	Catalyst loading (wt.%)	Ref.
60CNT	Micrometric bundles	99	10	36	2[a]	This work
Red mud	>100 nm	100	2	19	10	[33]
Fe onto biochar	80	99	15	54	10	[76]
Co/Al_2O_3	13	99	70	62	10	[79]
Fe nanoparticles	60	100	8	Not reported	12	[80]
Ni nanoparticles	<19	100	6	Not reported	10	[81]
Ni/MWCNTs	6	100	4	32	28	[70]
Cu supported onto zeolite	50	100	120	54	2	[75]
Ru/MWCNTs	12	100	1	32	5	[71]
Rh/Al_2O_3	3	100	2	21	2	[74]
PtO/MWCNTs	Not available	100	2	46	20	[72]
Ru/zeolite	1	100	8	67	0.5	[73]

[a]) calculated on wt.% of 60CNT added.

original draft, Visualization, Investigation, Formal analysis. **Candido Fabrizio Pirri:** Writing – review & editing, Writing – original draft, Validation, Supervision, Resources, Project administration, Funding acquisition. **Sergio Bocchini:** Writing – review & editing, Writing – original draft, Visualization, Validation, Supervision, Project administration, Investigation.

Declaration of competing interest

The authors declare that they have no known competing financial interests or personal relationships that could have appeared to influence the work reported in this paper.

Acknowledgements

This study was carried out within the Agritech National Research Center and received funding from the European Union Next-GenerationEU (PIANO NAZIONALE DI RIPRESA E RESILIENZA (PNRR) – MISSIONE 4 COMPONENTE 2, INVESTIMENTO 1.4 – D.D. 1032 17/06/2022, CN00000022). Furthermore, authors wish to thank European Union for the financial support through the Next Generation EU- Piano Nazionale Resistenza e Resilienza (PNRR) projects “Nord Ovest Digitale E Sostenibile-NODES” (PNRR, D.D. n.1054 23/06/2022) and NEST “ Network for Energy Sustainable Transition-NEST”(PE0000021, D.D. n.341 15/03/2022) and PNRR Mission 4 “Education and Research”—Component 2 “From research to business”—Investment 3.1 “Fund for the realization of an integrated system of research and innovation infrastructures”—Call for tender No. n. 3264 of 28/12/2021 of Italian Ministry of Research funded by the European Union—NextGenerationEU—Project code: IR0000027, Concession Decree No. 128 of 21/06/2022 adopted by the Italian Ministry of Research, CUP: B33C22000710006, Project title: iENTRANCE. The authors also acknowledge Ministero dello Sviluppo Economico (MISE) and Ministero della Transizione Ecologica (MITE) for the financial support. This manuscript reflects only the authors’ views and opinions, neither the European Union nor the European Commission can be considered responsible for them.

Appendix A. Supplementary data

Supplementary data to this article can be found online at https://doi.org/10.1016/j.apsusc.2025.164800.

Data availability

Data will be made available on request.

References

[1] C. Acar, I. Dincer, Review and evaluation of hydrogen production options for better environment, J. Clean. Prod. 218 (2019) 835–849.
[2] A.G. Cardone, M. Bartoli, A. Sacco, C.F. Pirri, M. Etzi, Microwave-Assisted Synthesis of Ir-Ni Electrocatalysts for the Oxygen Evolution Reaction in Acidic Electrolyte, ChemistryOpen, 2500279.
[3] M. Etzi Coller Pascuzzi, J.P. Hofmann, E.J.M. Hensen, Promoting oxygen evolution of IrO2 in acid electrolyte by Mn, Electrochimica Acta, 366 (2021) 137448.
[4] M. Etzi Coller Pascuzzi, M. van Velzen, J.P. Hofmann, E.J. Hensen, On the stability of Co3O4 oxygen evolution electrocatalysts in acid, ChemCatChem, 13 (2021) 459-467.
[5] M.E.C. Pascuzzi, A.J. Man, A. Goryachev, J.P. Hofmann, E.J. Hensen, Investigation of the stability of NiFe-(oxy) hydroxide anodes in alkaline water electrolysis under industrially relevant conditions, Cat. Sci. Technol. 10 (2020) 5593–5601.
[6] M.R. Usman, Hydrogen storage methods: Review and current status, Renew. Sustain. Energy Rev. 167 (2022) 112743.
[7] S. Krasae-in, J.H. Stang, P. Neksa, Development of large-scale hydrogen liquefaction processes from 1898 to 2009, International Journal of Hydrogen Energy, 35 (2010) 4524-4533.
[8] O.o.E.E.a.R. Energy, Hydrogen Storage, in, 2022.
[9] T. Michler, M. Lindner, U. Eberle, J. Meusinger, Assessing hydrogen embrittlement in automotive hydrogen tanks, in: Gaseous hydrogen embrittlement of materials in energy technologies, Elsevier, 2012, pp. 94-125.
[10] T. Brunner, M. Kampitsch, O. Kircher, Cryo-compressed hydrogen storage, Fuel cells: data, facts, and figures, (2016) 162-172.
[11] A.N. Laboratory, Technical Assessment of Cryo-Compressed Hydrogen Storage Tank Systems for Automotive Applications, in, Oak Ridge, TN, U.S., 2099.
[12] A. Züttel, C. Nützenadel, P. Sudan, P. Mauron, C. Emmenegger, S. Rentsch, L. Schlapbach, A. Weidenkaff, T. Kiyobayashi, Hydrogen sorption by carbon nanotubes and other carbon nanostructures, J. Alloy. Compd. 330 (2002) 676–682.
[13] S.J. Yang, H. Jung, T. Kim, C.R. Park, Recent advances in hydrogen storage technologies based on nanoporous carbon materials, Prog. Nat. Sci.: Mater. Int. 22 (2012) 631–638.
[14] S. Meduri, J. Nandanavanam, Materials for hydrogen storage at room temperature–An overview, Materials Today: Proceedings, (2022).
[15] N.L. Rosi, J. Eckert, M. Eddaoudi, D.T. Vodak, J. Kim, M. O'Keeffe, O.M. Yaghi, Hydrogen Storage in Microporous Metal-Organic Frameworks, Science 300 (2003) 1127–1129.
[16] P. Bénard, R. Chahine, Storage of hydrogen by physisorption on carbon and nanostructured materials, Scr. Mater. 56 (2007) 803–808.
[17] E. Klontzas, E. Tylianakis, G.E. Froudakis, Hydrogen storage in 3D covalent organic frameworks, A Multiscale Theoretical Investigation, the Journal of Physical Chemistry C 112 (2008) 9095–9098.
[18] T.L. LeValley, A.R. Richard, M. Fan, The progress in water gas shift and steam reforming hydrogen production technologies–a review, Int. J. Hydrogen Energy 39 (2014) 16983–17000.
[19] A.M. Amin, E. Croiset, W. Epling, Review of methane catalytic cracking for hydrogen production, Int. J. Hydrogen Energy 36 (2011) 2904–2935.
[20] M. Aziz, A.T. Wijayanta, A.B.D. Nandiyanto, Ammonia as effective hydrogen storage: a review on production, storage and utilization, Energies 13 (2020) 3062.
[21] M. Amende, C. Gleichweit, K. Werner, S. Schernich, W. Zhao, M.P. Lorenz, O. Höfert, C. Papp, M. Koch, P. Wasserscheid, Model catalytic studies of liquid organic hydrogen carriers: dehydrogenation and decomposition mechanisms of dodecahydro-N-ethylcarbazole on Pt (111), ACS Catal. 4 (2014) 657–665.
[22] F. Sotoodeh, K.J. Smith, An overview of the kinetics and catalysis of hydrogen storage on organic liquids, Can. J. Chem. Eng. 91 (2013) 1477–1490.
[23] L. Shi, S. Qi, J. Qu, T. Che, C. Yi, B. Yang, Integration of hydrogenation and dehydrogenation based on dibenzyltoluene as liquid organic hydrogen energy carrier, Int. J. Hydrogen Energy 44 (2019) 5345–5354.
[24] Z. Ding, S. Li, Y. Zhou, Z. Chen, W. Yang, W. Ma, L. Shaw, LiBH4 for hydrogen storage-new perspectives, Nano Mater. Sci. 2 (2020) 109–119.
[25] C. Webb, A review of catalyst-enhanced magnesium hydride as a hydrogen storage material, J. Phys. Chem. Solid 84 (2015) 96–106.

[26] M.B. Ley, L.H. Jepsen, Y.-S. Lee, Y.W. Cho, J.M.B. Von Colbe, M. Dornheim, M. Rokni, J.O. Jensen, M. Sloth, Y. Filinchuk, Complex hydrides for hydrogen storage–new perspectives, Mater. Today 17 (2014) 122–128.
[27] U.B. Demirci, Ammonia borane, a material with exceptional properties for chemical hydrogen storage, Int. J. Hydrogen Energy 42 (2017) 9978–10013.
[28] P. Wang, Solid-state thermolysis of ammonia borane and related materials for high-capacity hydrogen storage, Dalton Trans. 41 (2012) 4296–4302.
[29] M. Bartoli, C.F. Pirri, S. Bocchini, Unraveling the effect of Carbon Nanotube Oxidation on Solid-State Decomposition of Ammonia Borane/Carbon Nanotube Composites, J. Phys. Chem. C 126 (2022) 16587–16594.
[30] C. Astorino, E. De Nardo, S. Lettieri, G. Ferraro, M. Bartoli, M. Etzi, A.M. Chiodoni, C.F. Pirri, S. Bocchini, Investigation of solid-state thermal decomposition of ammonia borane mix with sulphonated poly (ellagic acid) for hydrogen release, Polymers 16 (2024) 3471.
[31] U. Sanyal, U.B. Demirci, B.R. Jagirdar, P. Miele, Hydrolysis of ammonia borane as a hydrogen source: fundamental issues and potential solutions towards implementation, ChemSusChem 4 (2011) 1731–1739.
[32] G. Gianola, M. Bartoli, C.F. Pirri, S. Bocchini, Hydrogen evolution through ammonia borane hydrolysis over iron tailored pig manure catalyst, Int. J. Hydrogen Energy 51 (2024) 21–28.
[33] M. Bartoli, M. Etzi, S. Lettieri, G. Ferraro, C.F. Pirri, A.M. Chiodoni, S. Bocchini, Complex Waste Stream utilization for Hydrogen Evolution: Ammonia Borane Hydrolysis over Red Mud Catalyst under Mild Conditions, Catal. Lett. 155 (2025) 1–9.
[34] A.C. Gangal, P. Sharma, Kinetic analysis and modeling of thermal decomposition of ammonia borane, Int. J. Chem. Kinet. 45 (2013) 452–461.
[35] C. Wang, J. Zhao, X. Du, S. Sun, X. Yu, X. Zhang, Z. Lu, L. Li, X. Yang, Hydrogen production from ammonia borane hydrolysis catalyzed by non-noble metal-based materials: a review, J. Mater. Sci. 56 (2021) 2856–2878.
[36] W. Ren, S. Liu, Y. Wang, J. Xie, C. Wan, L. Xu, S. Li, J. Wang, P.S. Postnikov, Sea urchin-like NiPt/TiCeO2 catalyst for rapid and efficient hydrogen production from hydrous hydrazine, J. Rare Earths (2025).
[37] C. Wan, R. Li, J. Wang, D.g. Cheng, F. Chen, L. Xu, M. Gao, Y. Kang, M. Eguchi, Y. Yamauchi, Silica confinement for stable and magnetic Co− Cu alloy nanoparticles in nitrogen-doped carbon for enhanced hydrogen evolution, Angewandte Chemie, 136 (2024) e202404505.
[38] C. Wan, G. Li, J. Wang, L. Xu, D.g. Cheng, F. Chen, Y. Asakura, Y. Kang, Y. Yamauchi, Modulating electronic metal-support interactions to boost visible-light-driven hydrolysis of ammonia borane: nickel-platinum nanoparticles supported on phosphorus-doped titania, Angewandte Chemie International Edition, 62 (2023) e202305371.
[39] S.-Y. Liu, W.-T. Ren, L.-Y. Chen, J. Xie, C. Wan, L.-X. Xu, S.-L. Li, J.-P. Wang, P. S. Postnikov, D.-G. Cheng, Constructing urchin-like TiO2 integrated NiPt nanoparticles for boosting the decomposition of hydrazine hydrate: S.-Y. Liu et al, Rare Met. (2025) 1–12.
[40] H.-L. Jiang, Q. Xu, Catalytic hydrolysis of ammonia borane for chemical hydrogen storage, Catal. Today 170 (2011) 56–63.
[41] T. Umegaki, Q. Xu, Y. Kojima, Porous materials for hydrolytic dehydrogenation of ammonia borane, Materials 8 (2015) 4512–4534.
[42] C. Wan, X. Liu, J. Wang, F. Chen, D.-G. Cheng, Heterostructuring 2D Co2P nanosheets with 0D CoP via a salt-assisted strategy for boosting hydrogen evolution from ammonia borane hydrolysis, Nano Res. 16 (2023) 6260–6269.
[43] H.-Z. Wang, Y.-X. Shao, Y.-F. Feng, Y.-J. Tan, Q.-Y. Liao, X.-D. Chen, X.-F. Zhang, Z.-H. Guo, H. Li, Heterostructured Co3O4–SnO2 composites containing oxygen vacancy with high activity and recyclability toward NH3BH3 dehydrogenation, Rare Met. 42 (2023) 3013–3023.
[44] Y. Li, J. Liao, Y. Feng, J. Li, Q. Liu, W. Zhou, M. He, H. Li, Built-in electric field in yolk shell CuO-Co3O4@ Co3O4 with modulated interfacial charge to facilitate hydrogen production from ammonia borane methanolysis under visible light, Adv. Funct. Mater. 34 (2024) 2405361.
[45] J. Liao, Y. Shao, Y. Feng, J. Zhang, C. Song, W. Zeng, J. Tang, H. Dong, Q. Liu, H. Li, Interfacial charge transfer induced dual-active-sites of heterostructured Cu0. 8Ni0. 2WO4 nanoparticles in ammonia borane methanolysis for fast hydrogen production, Appl Catal B 320 (2023) 121973.
[46] J. Liao, Y. Wu, Y. Shao, Y. Feng, X. Zhang, W. Zhang, J. Li, M. Wu, H. Dong, Q. Liu, Ammonia borane methanolysis for hydrogen evolution on Cu3Mo2O9/NiMoO4 hollow microspheres, Chem. Eng. J. 449 (2022) 137755.
[47] H. Li, Y. Yan, S. Feng, Y. Chen, H. Fan, Ammonia borane and its applications in the advanced energy technology, J. Energy Res. Technol. 143 (2021) 110801.
[48] R. Andrews, D. Jacques, D. Qian, E.C. Dickey, Purification and structural annealing of multiwalled carbon nanotubes at graphitization temperatures, Carbon 39 (2001) 1681–1687.
[49] A. Tagliaferro, M. Rovere, E. Padovano, M. Bartoli, M. Giorcelli, Introducing the novel mixed gaussian-lorentzian lineshape in the analysis of the raman signal of biochar, Nanomaterials 10 (2020) 1–19.
[50] A. Abutaleb, N. Zouli, M. El-Halwany, M. Ubaidullah, A. Yousef, Graphitic nanofibers supported NiMn bimetallic nanoalloys as catalysts for H2 generation from ammonia borane, Int. J. Hydrogen Energy 46 (2021) 35248–35260.
[51] N. Mohajeri, T. Ali, O. Adebiyi, Hydrolytic cleavage of ammonia-borane complex for hydrogen production, J. Power Sources 167 (2007) 482–485.
[52] S. Chernyak, A. Ivanov, N. Strokova, K. Maslakov, S. Savilov, V. Lunin, Mechanism of thermal defunctionalization of oxidized carbon nanotubes, J. Phys. Chem. C 120 (2016) 17465–17474.
[53] A. Orlando, F. Franceschini, C. Muscas, S. Pidkova, M. Bartoli, M. Rovere, A. Tagliaferro, A comprehensive review on Raman spectroscopy applications, Chemosensors 9 (2021).
[54] F. Tuinstra, J.L. Koenig, Raman Spectrum of Graphite, J. Chem. Phys. 53 (1970) 1126–1130.
[55] N. Shimodaira, A. Masui, Raman spectroscopic investigations of activated carbon materials, J. Appl. Phys. 92 (2002) 902–909.
[56] R. Arrigo, M. Bartoli, G. Malucelli, Poly(lactic Acid)-biochar biocomposites: effect of processing and filler content on rheological, thermal, and mechanical properties, Polymers 12 (2020).
[57] M. Bartoli, D. Duraccio, M.G. Faga, E. Piatti, D. Torsello, G. Ghigo, G. Malucelli, Mechanical, electrical, thermal and tribological behavior of epoxy resin composites reinforced with waste hemp-derived carbon fibers, J. Mater. Sci. 57 (2022) 14861–14876.
[58] M. Bartoli, M. Giorcelli, C. Rosso, M. Rovere, P. Jagdale, A. Tagliaferro, Influence of commercial biochar fillers on brittleness/ductility of epoxy resin composites, Applied Sciences (switzerland) 9 (2019).
[59] M. Bartoli, M.A. Nasir, P. Jagdale, E. Passaglia, R. Spiniello, C. Rosso, M. Giorcelli, M. Rovere, A. Tagliaferro, Influence of pyrolytic thermal history on olive pruning biochar and related epoxy composites mechanical properties, J. Compos. Mater. 54 (2020) 1863–1873.
[60] M. Bartoli, D. Torsello, E. Piatti, M. Giorcelli, A.C. Sparavigna, M. Rovere, G. Ghigo, A. Tagliaferro, Pressure-Responsive Conductive Poly(vinyl alcohol) Composites Containing Waste Cotton Fibers Biochar, Micromachines 13 (2022).
[61] M. Bartoli, M. Troiano, P. Giudicianni, D. Amato, M. Giorcelli, R. Solimene, A. Tagliaferro, Effect of heating rate and feedstock nature on electrical conductivity of biochar and biochar-based composites, Appl. Energy Combust. Sci. 12 (2022).
[62] A. Bifulco, M. Bartoli, I. Climaco, M.C. Franchino, D. Battegazzore, R.A. Mensah, O. Das, H. Vahabi, G. Malucelli, A. Aronne, C. Imparato, Coffee waste-derived biochar as a flame retardant for epoxy nanocomposites, Sustain. Mater. Technol. 41 (2024).
[63] S. Lepak-Kuc, M. Kiciński, P.P. Michalski, K. Pavlov, M. Giorcelli, M. Bartoli, M. Jakubowska, Innovative biochar-based composite fibres from recycled material, Materials 14 (2021).
[64] D. Torsello, M. Bartoli, M. Giorcelli, M. Rovere, R. Arrigo, G. Malucelli, A. Tagliaferro, G. Ghigo, High frequency electromagnetic shielding by biochar-based composites, Nanomaterials 11 (2021).
[65] D. Torsello, G. Ghigo, M. Giorcelli, M. Bartoli, M. Rovere, A. Tagliaferro, Tuning the microwave electromagnetic properties of biochar-based composites by annealing, Carbon Trends 4 (2021).
[66] F.C. Tai, C. Wei, S.H. Chang, W.S. Chen, Raman and X-ray diffraction analysis on unburned carbon powder refined from fly ash, J. Raman Spectrosc. 41 (2010) 933–937.
[67] D.N. Futaba, T. Yamada, K. Kobashi, M. Yumura, K. Hata, Macroscopic wall number analysis of single-walled, double-walled, and few-walled carbon nanotubes by X-ray diffraction, J. Am. Chem. Soc. 133 (2011) 5716–5719.
[68] Z. Wu, Y. Duan, S. Ge, A.C. Yip, F. Yang, Y. Li, T. Dou, Promoting hydrolysis of ammonia borane over multiwalled carbon nanotube-supported Ru catalysts via hydrogen spillover, Catal. Commun. 91 (2017) 10–15.
[69] P. Xu, W. Lu, J. Zhang, L. Zhang, Efficient hydrolysis of ammonia borane for hydrogen evolution catalyzed by plasmonic Ag@ Pd core–shell nanocubes, ACS Sustain. Chem. Eng. 8 (2020) 12366–12377.
[70] J. Zhang, C. Chen, W. Yan, F. Duan, B. Zhang, Z. Gao, Y. Qin, Ni nanoparticles supported on CNTs with excellent activity produced by atomic layer deposition for hydrogen generation from the hydrolysis of ammonia borane, Cat. Sci. Technol. 6 (2016) 2112–2119.
[71] C. Liu, D. Wei, C. Yin, S. Qiu, Y. Xia, Y. Zou, F. Xu, L. Sun, H. Chu, Ruthenium nanoparticles supported on functionalized carbon nanotubes as high-efficiency catalysts for ammonia borane hydrolysis, Mater. Chem. Phys. 319 (2024) 129398.
[72] W. Chen, D. Li, Z. Wang, G. Qian, Z. Sui, X. Duan, X. Zhou, I. Yeboah, D. Chen, Reaction mechanism and kinetics for hydrolytic dehydrogenation of ammonia borane on a Pt/CNT catalyst, AIChE J 63 (2017) 60–65.
[73] M. Zahmakıran, S. Özkar, Zeolite framework stabilized rhodium (0) nanoclusters catalyst for the hydrolysis of ammonia-borane in air: outstanding catalytic activity, reusability and lifetime, Appl Catal B 89 (2009) 104–110.
[74] M. Chandra, Q. Xu, Room temperature hydrogen generation from aqueous ammonia-borane using noble metal nano-clusters as highly active catalysts, J. Power Sources 168 (2007) 135–142.
[75] M. Zahmakıran, F. Durap, S. Özkar, Zeolite Confined Copper (0) Nanoclusters as Cost-Effective and Reusable Catalyst in Hydrogen Generation from the Hydrolysis of Ammonia-Borane, International Journal of Hydrogen Energy 35 (2010) 187–197.
[76] G. Gianola, M. Bartoli, C.F. Pirri, S. Bocchini, Hydrogen evolution through ammonia borane hydrolysis over iron tailored pig manure catalyst, Int. J. Hydrogen Energy 51 (2023) 21–28.
[77] B.C. Filiz, A.K. Figen, S. Pişkin, Applied ultrasound assisted research on synthesis and in-situ hydrolysis of ammonia borane for hydrogen energy, Int. J. Hydrogen Energy 44 (2019) 10003–10013.
[78] W. Li, Y. Shen, L. Dai, C. An, Strong Electronic Metal–Support Interaction Augments Hydrogen Evolution over hcp-Ni/In2O3 with Ultrasound-Assisting Dehydrogenation of Ammonia Borane, Energy Fuel 37 (2023) 8699–8706.

[79] Q. Xu, M. Chandra, Catalytic activities of non-noble metals for hydrogen generation from aqueous ammonia–borane at room temperature, J. Power Sources 163 (2006) 364–370.
[80] J.M. Yan, X.B. Zhang, S. Han, H. Shioyama, Q. Xu, Iron-nanoparticle-catalyzed hydrolytic dehydrogenation of ammonia borane for chemical hydrogen storage, Angew. Chem. Int. Ed. 47 (2008) 2287–2289.
[81] J.-M. Yan, X.-B. Zhang, S. Han, H. Shioyama, Q. Xu, Synthesis of longtime water/air-stable Ni nanoparticles and their high catalytic activity for hydrolysis of ammonia– borane for hydrogen generation, Inorg. Chem. 48 (2009) 7389–7393.